

Steady CFD simulation of central vortex formation at the free surface in the vessel without baffles stirred by impeller with three curved blades

Ing. Petr Vlček

Supervisor: prof. Ing. Tomáš Jirout, Ph.D.

Abstract

This work deals with the numerical simulation of fluid flow (for tested case water was applied) in the vessel without baffles focusing on the creation of the vortex and its shape on the free surface. The vessel is stirred by impeller with three curved blades with particular geometry. CFD program ANSYS FLUENT is used for the simulations. Steady flow regime is assumed. SST k-omega and Reynolds Stress turbulent models are used for the simulation of turbulence and MRF approach is used for simulation of impeller motion. VOF model is used to solve multiphase flow.

The one geometry of stirred vessel without baffles is solved and the sensitivity analyses of mesh roughness were performed. Higher rotation speeds from 200 to 350 rpm are set to establish a large central vortex. Further experiments were carried out with the same geometry.

The shapes of vortices and flow fields are compared for different meshes and turbulent models. Furthermore, the value of power numbers and depth of vortices are compared.

The results showed that application of two-equation turbulent models isn't suitable in this case. Despite the good convergence of the SST k-omega model its solution isn't correct and the shape of vortex doesn't correspond with experiment. More realistic shape of the central vortex is achieved by using the model Reynolds Stress, which has worse convergence, but it is preferable in cases, where is the dominant anisotropic turbulence (strong central vortex). Power number obtained by simulations with the model Reynolds Stress coincides with the value obtained by experiment.

The results also showed that the obtained shapes of vortices and flow fields aren't significantly sensitive to mesh roughness. Also power numbers are almost identical. Mesh roughness has the effect on the sharpness of the interface between phases, therefore it is appropriate to use finer mesh where place of the interface is expected.

Key words

Numeric simulation, CFD, FLUENT, Mixing, Stirred vessel, Free surface, Vortex, VOF

1. Introduction

This work deals with the numerical simulation of fluid flow (water was applied) in the vessel without baffles. In this case the liquid substantially rotates and creates a well observable central vortex. The aim of the work is to obtain the correct shape and depth of the vortex using the steady flow CFD simulation. The experiments will be carried out on a model device with the same geometry, where the higher speeds of impeller in a range from 200 rpm to 350 rpm will be set, and it will be the same as in the simulations. The central vortex establishment is guaranteed and air suction to the batch is avoided in arranged

revolution range. The shape of the vortex will be recorded by the camera and its depth will be measured manually by linear meter. A power characteristic will be also measured. It will be recommended the most reliable numerical model of steady flow, of which results best matches the experiments.

2. Problem analysis

In terms of flow simulation the stirred vessel is a special case. In this case it is necessary to ensure the movement of the impeller in the vessel and adjust the boundary conditions of the problem. There are no water inlets or outflows in the model.

We will consider a 3D geometric model for steady flow regime. The flow is turbulent. In this case, it is possible to use any of the two-equation turbulence models, or seven-equation model of Reynolds stresses.

Turbulence model SST $k-\omega$ will be selected from the two-equation models, which has the advantage of lower computational demands. This is the most modern model of two-equation turbulence models available in FLUENT. Model SST $k-\omega$ combines the robustness and accuracy of the $k-\omega$ model in areas close to the wall with the $k-\epsilon$ which works better in free flow.

The Reynolds stress model (RSM) is the most elaborated type of RANS turbulence model that ANSYS FLUENT provides. This model has significant demands on computing time, not only because of the large number of equations, but mainly because of convergence reduction. This additional effort is not always justified by increased accuracy compared to simpler two-equation models but for the flow at which strong swirl and rotation dominates, e.g. the case of stirred vessel without baffles using of this model is justified. The fact that this model doesn't use the isotropic turbulent viscosity, it has greater potential for these complex flow cases to achieve more accurate predictions than two-equation models.

The MRF (Multiple Reference Frames) approach will be used to simulate the rotation of the impeller that is suitable for solving the steady state. It requires division of the volume into two parts (rotary and stationary), where the rotary part contains an impeller.

VOF model will be used to solve multiphase flow. This model is suitable for solving the flow of immiscible fluids where it is necessary to monitor their interface.

3. Model geometry and mesh

Geometry for CFD simulation was created using ANSYS DesignModeler. Basic dimensions of the impeller and vessel are shown in Figure 1 and Table 1. The volume of the vessel was divided into rotary and the stationary part according to requirement of the MRF method. Further the geometry model is decomposed into sub-volumes to create semi-structured mesh, see Figure 1.

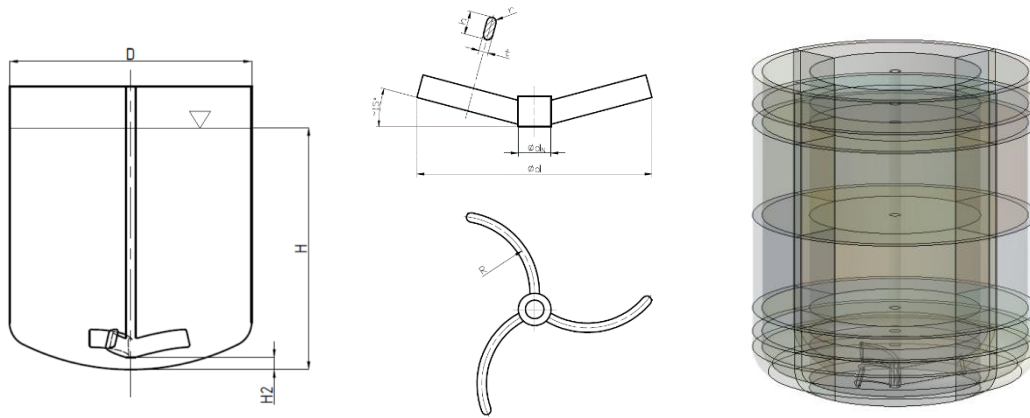


FIG. 1. Scheme and geometry of impeller and vessel, division of geometry model.

Table 1. Geometrical parameters and dimensions of the vessel and the impeller with curved blades.

D [mm]	H/D	D/d	H2/d	h/d	t/d	d [mm]	H2 [mm]	R [mm]	h [mm]	t [mm]
300	1	2	0.1	0.15	0.03	150	15	50	22.5	5

The computing mesh was created in ANSYS Meshing. The rotary volume which includes curved surfaces of impeller was meshed using tetrahedrons, stationary part using hexahedrons. Three computing meshes were created with the number of cells 460K, 630K, 800K in order to perform a sensitivity analysis on the mesh density.

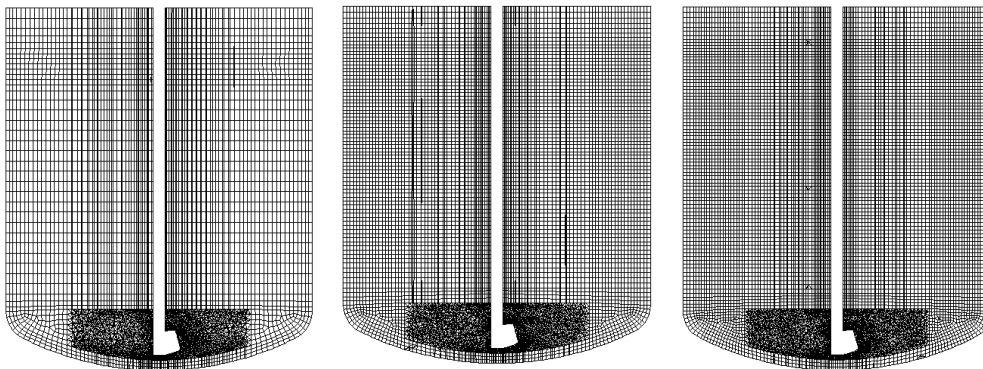


FIG 2. The cuts of created meshes. From left: 460K, 630K, 800K elements.

4. Processor setup and calculation

The solution was done in ANSYS FLUENT 14.5. The solver was set according to Tables 2 and 3.

Table 2. Solver setup for the case of stirred vessel with turbulence model SST k- ω

Turbulence model	SST k- ω
Fluids in the stirred vessel	water, air
Boundary conditions	rotation MRF (200 rpm) vessel top – pressure-outlet
Discretization – pressure	PRESTO!
Discretization – momentum	Second Order Upwind
Discretization – VOF	Compressive
Discretization – turbulent kinetic energy	Second Order Upwind
Discretization – turbulent dissipation rate	Second Order Upwind
Residuals	10E-05

Table 3. Solver setup for the case of stirred vessel with turbulence model Reynolds Stress

Turbulence model	Reynolds Stress; Quadratic Pressure-Strain
Fluids in the stirred vessel	water, air
Boundary conditions	rotation MRF (200 rpm) vessel top – pressure-outlet
Discretization – pressure	PRESTO!
Discretization – momentum	Second Order Upwind
Discretization – VOF	Compressive
Discretization – turbulent kinetic energy	Second Order Upwind
Discretization – turbulent dissipation rate	Second Order Upwind
Discretization – Reynolds Stresses	First Order Upwind
Residuals	10E-05

At first the calculation was carried out with a model SST k- ω with the lowest speed (200 rpm). The Reynolds Stress turbulence model was switched on after achieving convergence. After the end of calculation impeller speed were changed and carried out other simulations.

5. The simulation results

First, we compare the results of simulations of both turbulent models for all meshes at speed of 200 rpm. Vortex shapes (the fractional distribution of air and water) are shown in Figure 3. This figure shows that the shape of the vortex is not significantly affected by mesh density. It is evident that finer mesh reduces blurring interface between the phases. Furthermore, it is obvious the large difference in the shape of vortex, depending on the turbulence model. The figure shows that a more realistic shape is achieved by using a model Reynolds Stress (compared with experimental data). This result was expected because two-equation turbulence models are based on the Boussinesq hypothesis of turbulent viscosity whose drawback is that the turbulent viscosity is assumed to be an isotropic scalar quantity. This assumption is not satisfied in the solved case, because of the predominant single big vortex and thus anisotropic turbulence is occurred. As it can be seen from the figure, this deficiency was markedly shown on the resulting flow. Reynolds Stress Model solves

a transport equation for each component of the Reynolds stress tensor, so it describes this case much better, but it is computationally more demanding. Therefore only this turbulence model was selected for further calculations. The torques and power numbers are compared in Table 4. The power number is evaluated by equation 1.

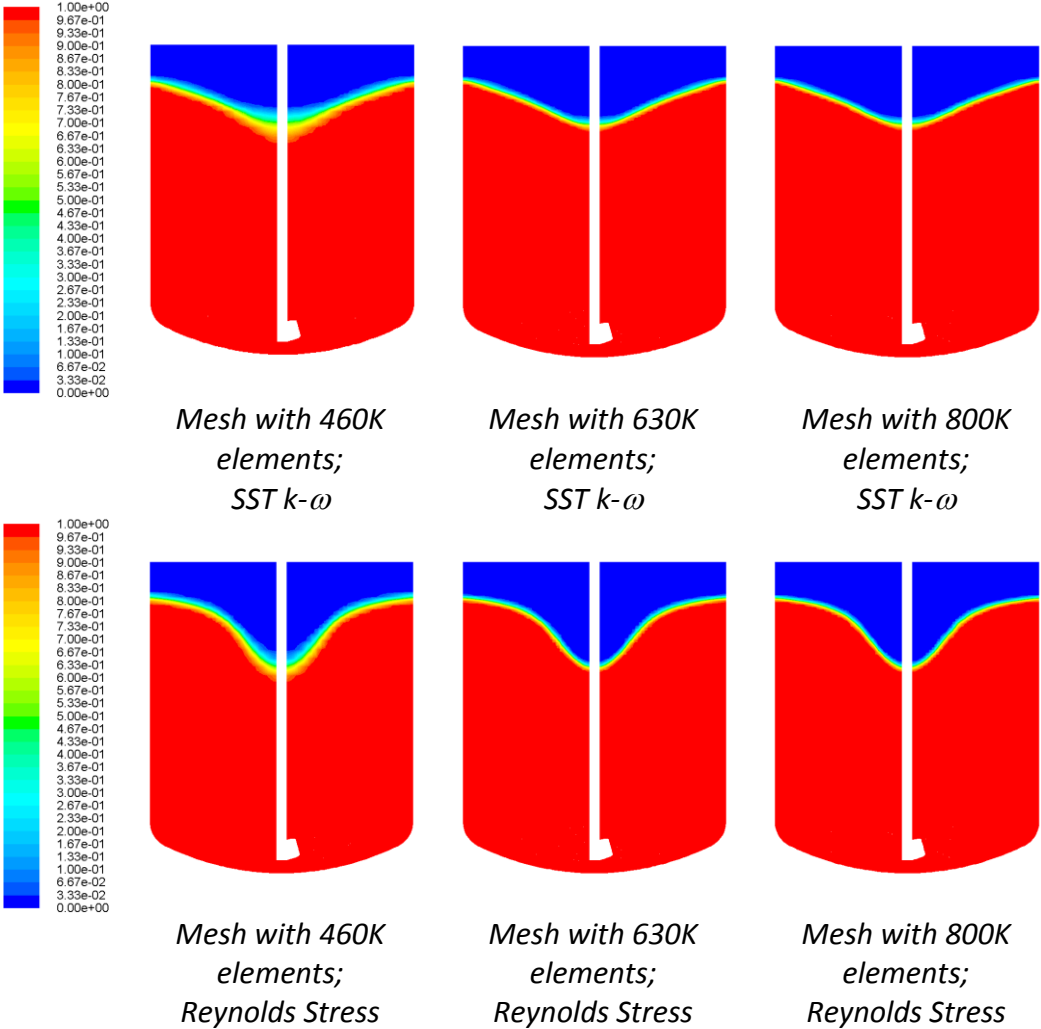


FIG. 3 Comparison of central vortex shapes at speed of 200 rpm for various coarse mesh and turbulence models SST $k-\omega$ and Reynolds Stress.

Table 4. The values of the torques of impeller and power numbers for speed 200 rpm.

Model	Mesh [10 ³ el.]	M _k [N.m]	P _o [-]
SST	460	0.05443	0.40606
	630	0.05574	0.41583
	800	0.05576	0.41598
RSM	460	0.03534	0.26364
	630	0.03616	0.26976
	800	0.03616	0.26976

$$P_o = \frac{2\pi M_K}{\rho n^2 d^5} \quad (1)$$

The table shows that in solved case where the anisotropic turbulence is predominant, two-equation model significantly fails also in determination of the torque. Differences between the torques or power numbers for each density of mesh are minimal. Torques for calculations with a model RSM and meshes with 630 and 800 thousand elements are same after rounding to five decimal places. Other characteristics will be compared for these two cases.

Figure 4 shows the velocity vectors and Figure 5 shows the pressure contours in the vertical cross-section of the vessel for the finer meshes. The figures show that the velocity field and the distribution of pressure in the vessel are almost identical. Also, the range of the scale is almost the same. The sensitivity analysis showed that the results didn't significantly depend on the coarseness of the mesh, only a greater blurring of the interface between the phases occurs with coarser mesh.

Therefore mesh with 630 thousand elements will be used for further calculations, where the blurring is not significantly larger than with the finer mesh and has the lower computational requirements.

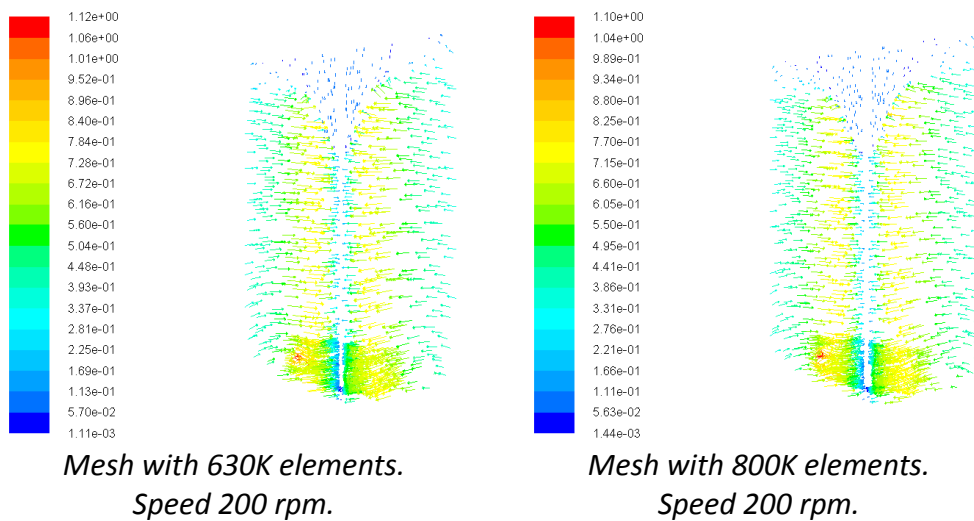


FIG. 4. Comparison of velocity vectors at speed of 200 rpm for various coarse meshes and turbulence model Reynolds Stress.

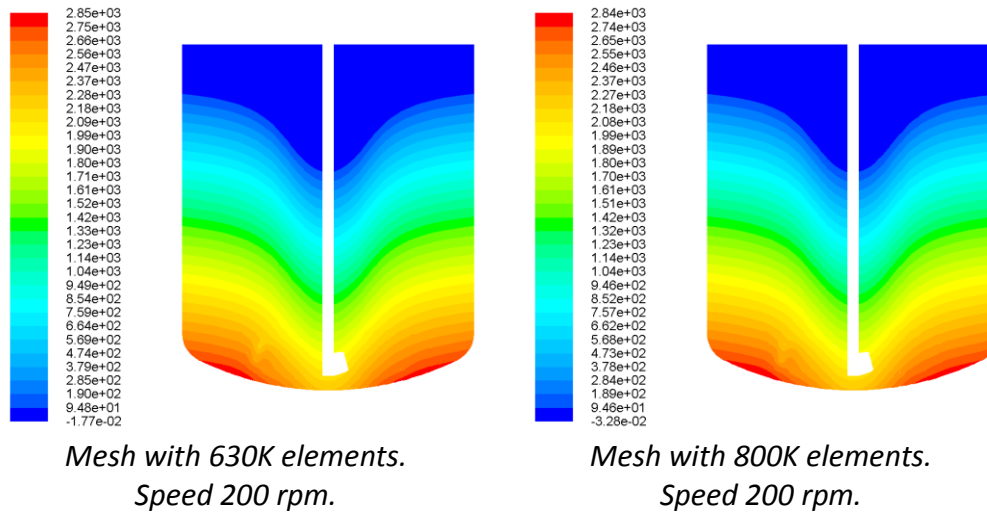


FIG. 5. Comparison of static pressure contours at speed of 200 rpm for various coarse meshes and turbulence model Reynolds Stress.

Figure 6 shows the change in the vortex high depending on speed in the range 200-350 rpm. The transition between phases is sharp enough. As was expected, the depth of the vortex increases with impeller speed.

Table 5. The values of the torque on the impeller and power numbers for different speeds, the distance of vortex bottom and top from the vessel bottom.

n [rpm]	Re [-]	Vortex bottom [m]	Vortex top [m]	Mk [N.m]	Po [-]
200	74865	0.235	0.314	0.0362	0.2698
210	78593	0.228	0.315	0.0398	0.2685
220	82335	0.221	0.317	0.0435	0.2678
230	86078	0.213	0.318	0.0475	0.2669
240	89820	0.205	0.32	0.0515	0.2669
250	93581	0.197	0.322	0.0559	0.2669
260	97325	0.189	0.323	0.0603	0.2662
270	101068	0.180	0.325	0.0651	0.2665
280	104811	0.171	0.327	0.0699	0.2659
290	108554	0.161	0.329	0.0751	0.2663
300	112298	0.151	0.331	0.0803	0.2663
310	116041	0.141	0.334	0.0857	0.2661
320	119784	0.130	0.336	0.0911	0.2656
330	123527	0.119	0.338	0.0968	0.2654
340	127271	0.107	0.340	0.1029	0.2656
350	131014	0.0958	0.343	0.1091	0.2658

Table 6. The results obtained with the mesh with 880 thousand elements. The values of the torque on the impeller and power numbers for different speeds, the distance of vortex bottom and top from the vessel bottom.

n [rpm]	Re [-]	Vortex bottom [m]	Vortex top [m]	Mk [N.m]	Po [-]
200	74865	0.235	0.313	0.0362	0.2698
250	93581	0.197	0.322	0.0559	0.2668
300	112298	0.150	0.331	0.0801	0.2655

Distances of the vortex global minimum and maximum high from the vessel bottom are shown in Table 5. The table contains also the moments acting on the impeller and calculated power numbers from them. Dimensions of vortex are determined in the place where the iso-surface of constant volume fraction of water with value 0.5 touches the impeller shaft in the middle of the vessel and where it touches the wall of the vessel.

From Table 5 it is evident that the power numbers are not very different and can be considered constant. This is consistent with the theory that the power number in the turbulent region is constant and doesn't depend on the impeller speed (on the Reynolds number). Table 6 shows the results obtained by simulation with finer mesh with 800 thousand elements cells. The obtained data are almost identical to the previous ones.

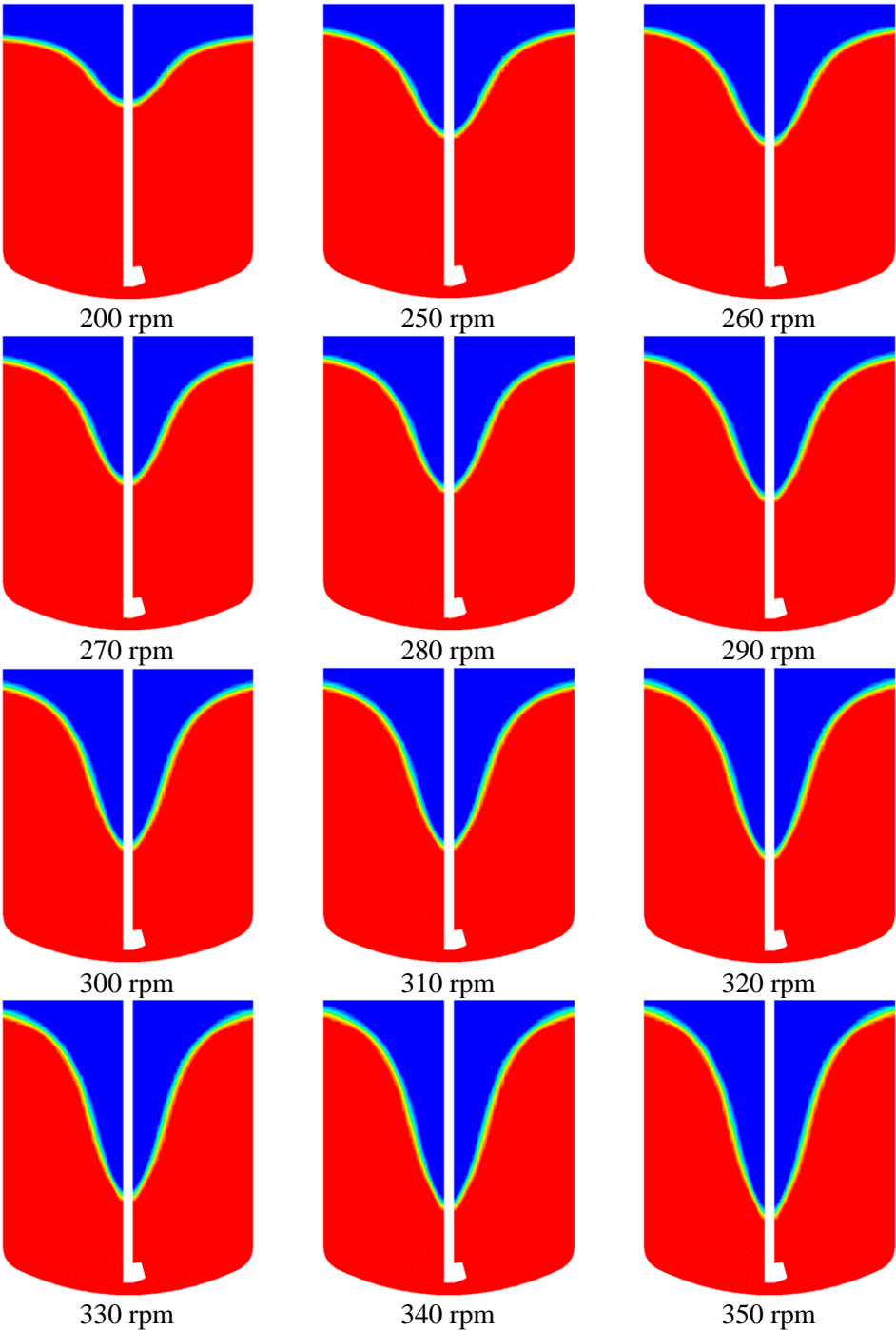


FIG. 6. The vortex shapes at different impeller speeds.

6. Experimental verification of simulations

Experiments were performed on a model device with the same geometry. In the experiment the shape of the vortex was monitored and recorded by camera. Its depth and height were also measured. Furthermore, the torque was measured with a torque sensor placed on the shaft. Data from the sensor were calibrated using a known six-blade impeller power characteristic.

Figure 6 and 7 shows graphs comparing the experimentally observed and simulated dimensions of vortex. The bottom of vortex was oscillated during measuring so minimum and maximum values were deducted.

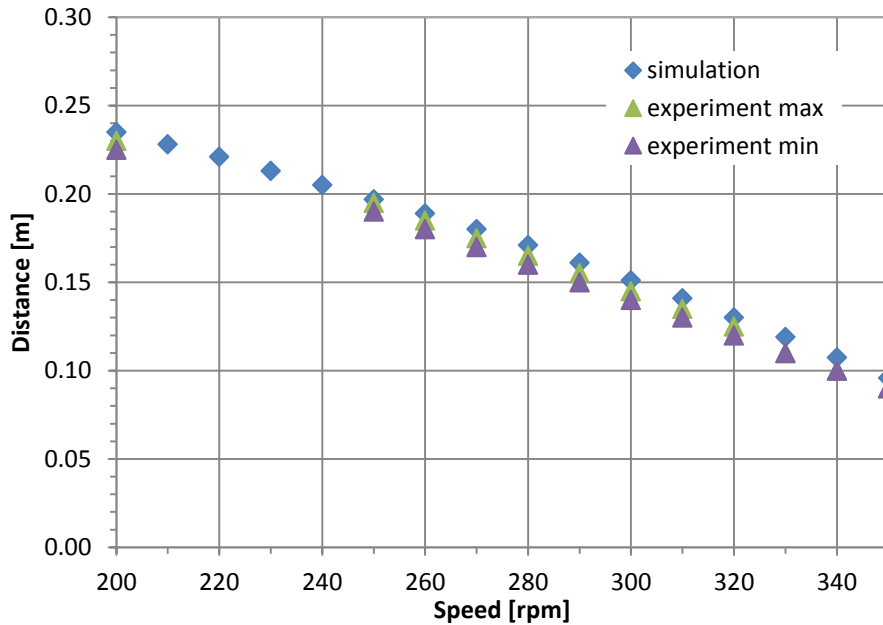


FIG. 6. The dependence of the distance of the vortex bottom from the vessel bottom on the impeller speed obtained by simulations and experiments.

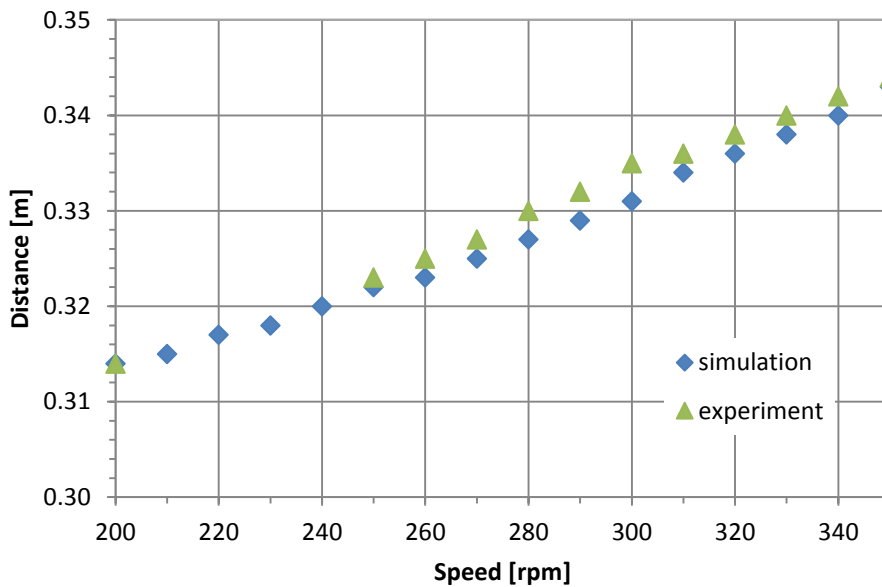


FIG. 7. The dependence of the distance of the vortex top from the vessel bottom on the impeller speed obtained by simulations and experiments.

The graph shows a similar trend of vortex sizes, but by the experiments vortex had about one centimetre bigger depth and its top part is therefore slightly higher. Differences may be due to the fact that in reality vortex oscillates and causes a small ripple on the surface and in the simulation the steady state is considered, i.e. the time-averaged values. The sizes of these differences are almost negligible. The vortex shapes obtained by simulations correspond very well with real vortex shapes. Comparison at the speed of 290 rpm is shown in Figure 8.

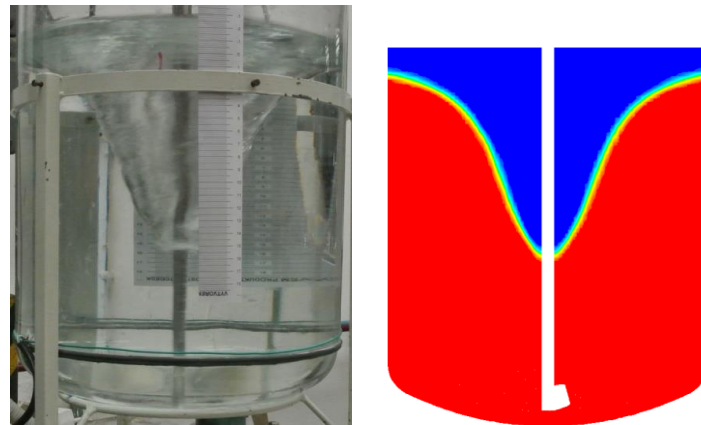


FIG. 8. The sample of comparison of the water surface shape obtained by numerical simulation with reality (290 rpm).

Experimentally determined and calculated torques acting on the impeller blades are graphically shown in Figure 9. Simulations and measurements have not been performed in gradually order. First, speed of 200, 250 and 300 rpm were set, after that the others were complemented. As it can be seen in Figure 9, the course of the torque simulated in random impeller speed hasn't been affected and torque curve has smooth course. But it had effect during experiment. Although it was always waited for sufficient time to achieve steady state conditions and torque was measured three times for each impeller speed, imperfection of measuring apparatus was reflected, and because not all speeds were measured sequentially, but at random sequence, torque waveform determined experimentally hasn't been so smooth. The graph shows that the measured and simulated data are in good agreement although to the simulation torques are slightly over predicted.

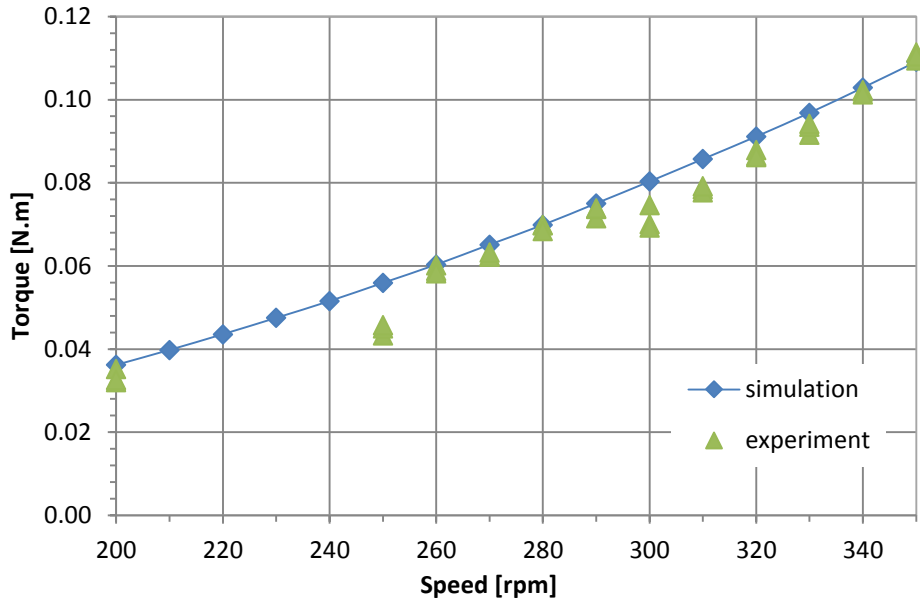


FIG. 9. Dependence of the torque on the impeller speed

Figure 10 shows the dependence of power numbers calculated from the torque on the impeller speed. It is seen that this dependence can be described by a constant, although the measured data have larger deviation. The average power number obtained by numerical simulation is approximately about 5.8% higher compared to the experiment. If probably inaccurately measured values for 200, 250 and 300 rpm would be omitted, the difference will be only 3.2%.

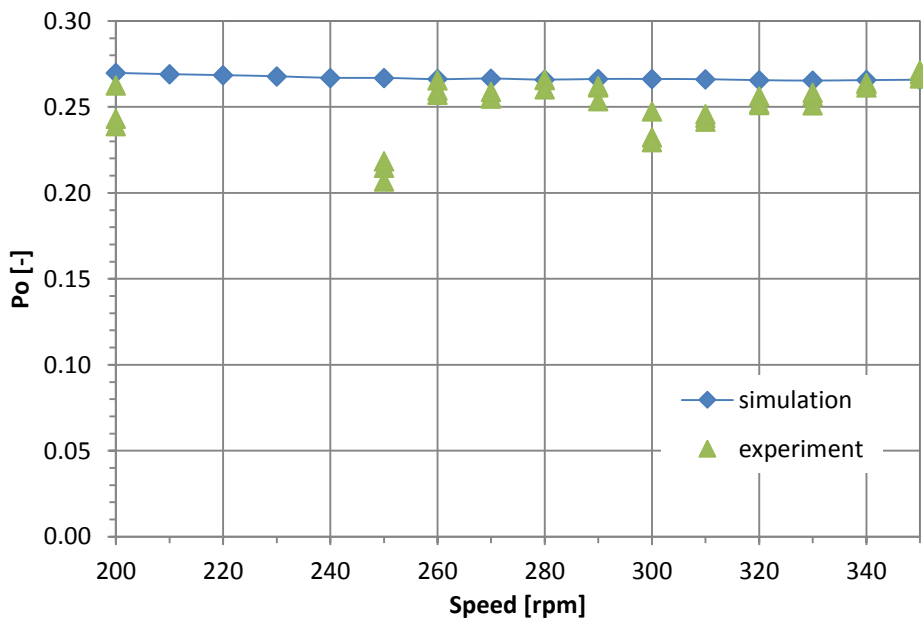


FIG. 10. Dependence of the power number on the impeller speed

These graphs are served to get an idea of achieved values for this particular case. The results in dimensionless form are shown in Figures 11 and 12 for more general use of results (similar geometry of different dimensions, impeller speed, different physical properties of the batch etc.). Dimensionless variables in figures are described in equations (2), (3) and (4).

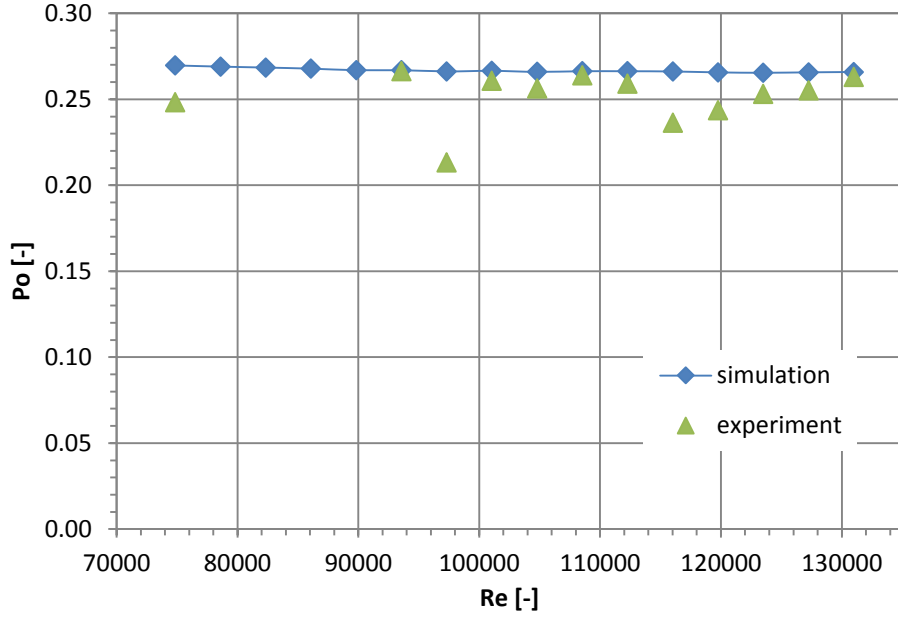


FIG. 11. Dependence of the power number on the Reynolds number

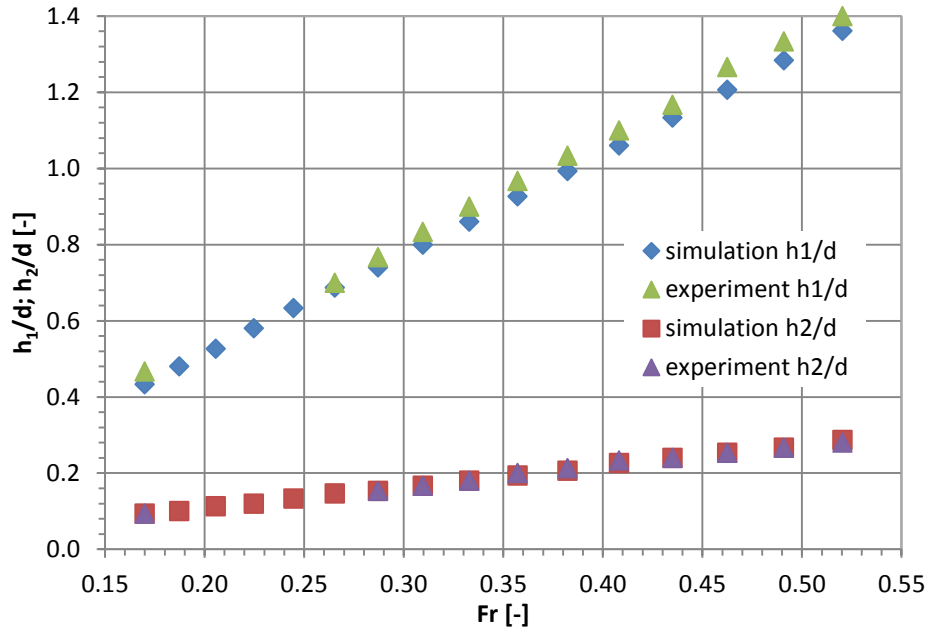


FIG. 12. Relative vortex depth h_1/d and relative elevation of liquid level at vessel wall h_2/d vs. Froude number Fr ;
 $Ga = 3.298 \times 10^{10}$, $D/d = 2$, $H_2/d = 0.1$

$$Re = \frac{nd^2\rho}{\mu} \quad (2)$$

$$Fr = \frac{n^2d}{g} \quad (3)$$

$$Ga = \frac{Re^2}{Fr} = \frac{\rho^2 d^3 g}{\mu^2} \quad (4)$$

7. Conclusion

A model was created for simulating the formation of vortex on the free water surface in a stirred vessel without baffles. The sensitivity analysis showed that the resulting flow didn't change much with coarseness of mesh. But coarseness of mesh has effect on the sharpness of the phase interface, therefore, it is appropriate to use finer grid at the place of expected interface.

The best turbulent model used for stationary simulation of stirred vessel without baffles is Reynolds Stress - Quadratic Pressure Strain. A good water surface shape was obtained with this model compared with the experiment. Prediction of the depth of vortex by simulation was about a centimetre smaller than that was found in the experiment, so average error is 5 %. Steady state wasn't achieved in the experiment. Depth of vortex fluctuated predominantly in the range of one centimetre, sometimes even more. Also water level on the top of vortex after some time rippled when impeller speeds were below 320 rpm.

Simulations found that in the solved range from 200 to 350 rpm power number is constant with a value of about 0.267. This value is about 5.8% higher than the average power number determined by experiment. Due to imperfections of the apparatus for measuring the torque on the shaft of the impeller and due to requirement to determine the absolute value of the torque by calibration of measurement data using a six-blade stirrer with a known power characteristic, result obtained by simulations can be considered as correct. A complicated geometry of the impeller would also cause inaccuracies, because manufactured impeller may not exactly match the model.

Acknowledgement

This research was supported by the Technology Agency of the Czech Republic under grant TA02011251 „*Optimization of enamelled mixing equipment according to technological needs of end users*“.

This work was supported by the Grant Agency of the Czech Technical University in Prague, grant No. SGS13/065.

This work was supported by the Grant Agency of the Czech Technical University in Prague, grant No. SGS14/135.

Symbols

D	-	Vessel diameter	[m]
d	-	Impeller diameter	[m]
Fr	-	Froude number	[-]
g	-	Gravitational acceleration	[m.s ⁻²]
Ga	-	Galileo number	[-]
H	-	Height of fluid surface	[m]
H ₂	-	Impeller distance from the bottom	[m]
h	-	Height of impeller blade	[m]
h ₁	-	Depth of liquid/gas interface at vessel axis with respect to static liquid surface level	[m]
h ₂	-	Elevation of liquid/gas interface at vessel wall with respect to static liquid surface level	[m]
t	-	Thickness of impeller blade	[m]
R	-	Radius of curvature blades	[m]
M _k	-	Torque	[N.m]
n	-	Rotation speed of impeller	[s ⁻¹]
P _o	-	Power number	[-]
Re	-	Reynolds number	[-]
μ	-	Dynamic viscosity	[Pa.s]
ρ	-	Density	[kg.m ⁻³]

Literature

- [1] ANSYS FLUENT Theory Guide, Release 14.5. ANSYS, Inc., October 2012.
- [2] ANSYS FLUENT User's Guide, Release 14.5. ANSYS, Inc., October 2012.
- [3] ANSYS Tutorials & Training Materials, Turbulence Flow Modeling using ANSYS FLUENT 14.0
- [4] ANSYS Tutorials & Training Materials, Multiphase Modeling in Fluent, Lecture 2 – Volume of Fluid Model
- [5] Vlček, P., Skočilas, J., Jirout, T.: *CFD simulace tvorby víru na volné hladině v nádobě bez narážek míchané třílopatkovým míchadlem se zakřivenými lopatkami*. In: *Sborník konference CHISA 2013*. Praha: Česká společnost chemického inženýrství, 2013, ISBN 978-80-02-02500-9.
- [6] Vlček, P., Skočilas, J., Jirout, T.: *Numerical simulation of fluid flow in a stirred vessel using FLUENT*. In: *PROCEEDINGS - 40th International Conference of Slovak Society of Chemical Engineering*. Bratislava: Slovak Society of Chemical Engineering, 2013, ISBN 978-80-89475-09-4.
- [7] Vlček, P., Skočilas, J., Jirout, T.: *Modelování turbulentního proudění*. In: *Procesní technika 2013*. Praha: České vysoké učení technické v Praze, Fakulta strojní, 2013, ISBN 978-80-01-05285-3.
- [8] Rieger, F., Ditzl, P., Novák, V.: *Vortex depth in mixed unbaffled vessels*. *Chemical Engineering Science*, 1979, Vol. 34, pp. 397-403.